Journal of Physics: Condensed Matter

PAPER

Emergence of intrinsic superconductivity below 1.178 K in the topologically non-trivial semimetal state of $CaSn_3$

To cite this article: Y L Zhu *et al* 2019 *J. Phys.: Condens. Matter* **31** 245703

IOP Publishing Journal of Physics: Condensed Matter
J. Phys.: Condens. Matter **31** (2019) 245703 (8pp) https://doi.org/10.1088/1361-648X/ab0f0d

Emergence of intrinsic superconductivity below 1.178 K in the topologically non-trivial semimetal state of $CaSn_3$

Y L Zhu[1], J Hu[1,2], F N Womack[3], D Graf[4], Y Wang[1], P W Adams[3] and Z Q Mao[1]

[1] Physics and Engineering Physics department, Tulane University, New Orleans, LA 70118, United States of America
[2] Department of Physics, University of Arkansas, Fayetteville, AR 72701, United States of America
[3] Department of Physics and Astronomy, Louisiana State University, Baton Rouge, LA 70803, United States of America
[4] National High Magnetic Field Laboratory, Tallahassee, FL 32310, United States of America

E-mail: jinhu@uark.edu and zmao@tulane.edu

Received 3 December 2018, revised 28 February 2019
Accepted for publication 12 March 2019
Published 4 April 2019

Abstract

Topological materials which are also superconducting are of great current interest, since they may exhibit a non-trivial topologically-mediated superconducting phase. Although there have been many reports of pressure-tuned or chemical-doping-induced superconductivity in a variety of topological materials, there have been few examples of intrinsic, ambient pressure superconductivity in a topological system having a stoichiometric composition. Here, we report that the pure intermetallic $CaSn_3$ not only exhibits topological fermion properties, but also has a superconducting phase at ~1.178 K under ambient pressure. The topological fermion properties, including the nearly zero quasi-particle mass and the non-trivial Berry phase accumulated in cyclotron motions, were revealed from the de Haas–van Alphen (dHvA) quantum oscillation studies of this material. Although $CaSn_3$ was previously reported to be superconducting with $T_c = 4.2$ K, our studies show that the $T_c = 4.2$ K superconductivity is extrinsic and caused by Sn on the degraded surface, whereas its intrinsic bulk superconducting transition occurs at 1.178 K. These findings make $CaSn_3$ a promising candidate for exploring new exotic states arising from the interplay between non-trivial band topology and superconductivity, e.g. topological superconductivity (TSC).

Keywords: superconductivity, topological materials, de Haas–van Alphen oscillation

S Supplementary material for this article is available online

(Some figures may appear in colour only in the online journal)

1. Introduction

Topological superconductivity (TSC) has attracted extensive interest due to its strong connection with Majorana fermions. Majorana fermions follow the Dirac equation and are particles which are their own antiparticles. The collective excitations on the surfaces of topological superconductors are believed to satisfy these conditions: the Dirac-like dispersion is guaranteed by the topological surface states (TSSs) and the particle-hole symmetry in the superconducting state results in indistinguishable electron and hole excitations. Therefore, the gapless surface states of a topological superconductor host Majorana fermions [1, 2]. TSC can be realized via the superconducting proximity effect in a superconductor-topological insulator [3–6] or superconductor-semiconductor hybrid structure [7–9]. Signatures of Majorana fermions have indeed been reported in such heterostructures [9–13]. In particular, half-integer quantized conductance plateaus

were recently observed in the quantum anomalous Hall insulator-superconductor hybrid system, suggesting 1D chiral Majorana fermion modes [13].

In addition to the proximity effect-induced TSC, several other strategies have been utilized to achieve TSC in bulk materials. One is to use chemical doping in topological insulators. This has produced signatures of TSC in some systems, e.g. $Cu_xBi_2Se_3$ [14–16]. Point contact, which is generally used for tunneling measurements, has also been found to generate possible TSC in the topological semimetal Cd_3As_2 [17, 18]. Another approach is to induce superconductivity in topological semimetals or insulators by applying high pressure [19–25]. However, it remains elusive whether such pressure-induced superconductivity is connected with TSC, since probing the Majorana surface modes of topological superconductors under pressure is a challenging task. In some cases, pressure is also likely to change the structure, thus resulting in trivial band topology [21]. These problems may be avoided by finding materials which display both non-trivial TSSs and intrinsic superconductivity at ambient pressure. Some materials have been found to show such properties, such as (Y/Lu)PtBi [26, 27], $PbTaSe_2$ [28–30], $FeTe_{0.55}Se_{0.45}$ [31], and β-$PdBi_2$ [32]. These materials not only have clear advantages for probing Majorana surface modes [30, 31], but also offer opportunities to observe new superconducting phenomena, such as unconventional superconductivity with spin-3/2 pairing in YPtBi [33]. These exciting advances underscore the importance of searching for other systems having a non-trivial band topology in conjunction with a bulk superconducting phase.

In this article, we report on the discovery of a new topological semimetal showing intrinsic superconductivity at ambient pressure, i.e. $CaSn_3$. This material possesses the $AuCu_3$-type cubic crystal structure with the space group $Pm\overline{3}m$. Recent first-principles calculations predicted a topologically non-trivial electronic state for this material [34]; without considering spin-orbital coupling (SOC), its electronic band structure is found to host a 3D topological nodal line state with a unique drumhead like TSSs protected by time reversal and mirror symmetries. When SOC is taken into account, each nodal line is predicted to evolve into two Weyl nodes [34]. This claim appears to conflict with a requirement for a Weyl state, i.e. either time reversal symmetry breaking or inversion symmetry breaking, since $CaSn_3$ does not satisfies either of these two requirements. Although this prediction needs to be further scrutinized, we have performed systematic quantum oscillation studies on this material through magnetic torque measurements, from which we indeed observed relativistic fermion behavior, suggesting $CaSn_3$ should possess non-trivial band topology. Furthermore, we find that this material shows intrinsic bulk superconductivity around 1.178 K, while the previously reported non-bulk superconducting transition at 4.2 K for this material [35] is extrinsic and caused by Sn present on its degraded surface. The presence of intrinsic superconductivity in a topologically non-trivial state makes $CaSn_3$ a promising new platform for the study of the interconnection between TSSs and superconductivity.

2. Experimental methods

$CaSn_3$ single crystals were synthesized using a self-flux method. The Ca pieces and Sn lumps were loaded into a baked Al_2O_3 crucible with the molar ratio of Ca/Sn = 1/4 and sealed in a quartz tube under high vacuum. The reagents were heated to 900 °C, kept at this temperature for 24 h and then slowly cooled down to 400 °C at a rate of 4 °C h^{-1}. The single crystals can be obtained after removing the unreacted Sn flux through centrifugation; the inset of figure 1(a) shows an optical image of a typical $CaSn_3$ crystal. The cubic shape of the obtained crystals is consistent with the face-centered cubic structure for $CaSn_3$ (figure 1(a)) [35], which is further confirmed by x-ray diffraction measurements (XRD) (see supplementary figure S1 (stacks.iop.org/JPhysCM/31/245703/mmedia)). Moreover, we also found $CaSn_3$ single crystals are air sensitive, consistent with the previous report [35]. When a sample is left in air for more than 30 min, the surface color changes dramatically. XRD measurements suggest that the degraded surface layer contains Sn as shown in supplementary figures S1 and 1(b) in [35], which causes the observation of the trace of superconductivity at 4.2 K, as will be discussed later. We have conducted magnetic torque measurements on $CaSn_3$ single crystals in a 31 T resistive magnet at the National High Magnetic Field Laboratory (NHMFL) in Tallahassee using a cantilever torque magnetometer. The specific heat of $CaSn_3$ single crystals was measured using the adiabatic thermal relaxation technique in the Physical Property Measurement System (Quantum Design).

3. Results

3.1. Relativistic fermion behavior in $CaSn_3$

We have observed strong dHvA oscillations in $CaSn_3$ single crystals in the magnetic torque measurements. In figure 1(b), we present the dHvA oscillation data for field nearly along the [1 0 0] direction (denoted as $B//[1\,0\,0]$). We chose such a field orientation for measurements, because the torque signal vanishes when the field is perfectly aligned normal or parallel to the surface of the cantilever tip where the sample is mounted. The dHvA oscillations start to appear from a field as low as 2 T at $T = 1.6$ K (see the inset to figure 1(b)), and remain visible at temperatures up to 80 K (figure 1(b)). Figure 1(c) presents the dHvA oscillation patterns after subtracting the non-oscillating background. Strong quantum oscillations at low fields and high temperatures generally imply high quantum mobility, which is verified by the quantitative analyses of the dHvA data as shown below. Furthermore, given the cubic crystal symmetry of $CaSn_3$, one can expect identical oscillation patterns for $B//[1\,0\,0]$ and $B//[0\,1\,0]$, which is indeed observed in our measurements, as shown in supplementary figure S2.

The oscillatory toque shown in figure 1(c) clearly displays multi-frequency components, as revealed by the fast Fourier transformation (FFT) analysis. As shown in figure 2(a), five major frequencies, i.e. $F_\alpha = 49$ T, $F_\beta = 59$ T, $F_\gamma = 347$ T, $F_\varepsilon = 463$ T and $F_\eta = 678$ T, can be resolved by the FFT

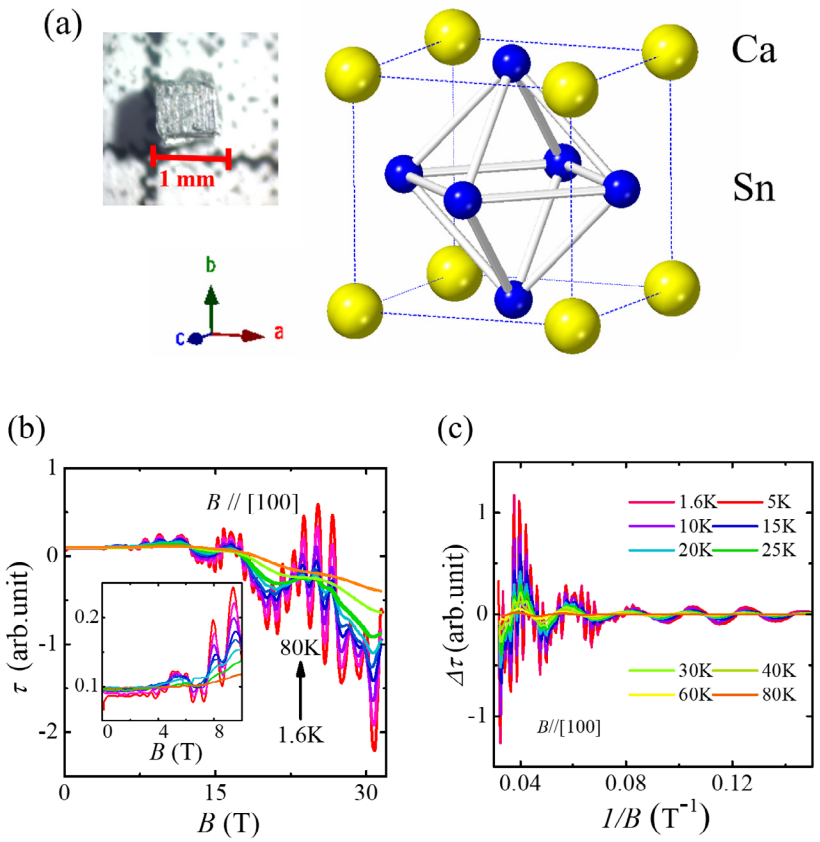

Figure 1. (a) Crystal structure of $CaSn_3$. Inset: an optical image of a $CaSn_3$ single crystal. (b) The field dependence of magnetic torque τ for $CaSn_3$ at different temperatures from 1.6 K to 80 K, which shows strong dHvA oscillations. The magnetic field is applied nearly along the [1 0 0] direction (B//[1 0 0]). Inset: enlarged low field oscillations. (c) The oscillatory components $\Delta\tau$ at different temperatures for B// [1 0 0].

analyses, implying a complex Fermi surface for $CaSn_3$. From further analysis of dHvA oscillations, we have found evidence for relativistic fermions in $CaSn_3$. In general, the oscillations of magnetization ΔM in a 3D topological semimetal can be described by the Lifshitz–Kosevich (LK) formula with a Berry phase being taken into account [36]:

$$\Delta M \propto -B^{\frac{1}{2}} R_T R_D R_S \sin[2\pi(\frac{F}{B} + \gamma - \delta)] \qquad (1)$$

where $R_T = \alpha T\mu/B\sinh(\alpha T\mu/B)$, $R_D = \exp(-\alpha T_D\mu/B)$ and $R_S = \cos(\pi g\mu/2)$. Here $\mu = m^*/m_0$ is the ratio of effective cyclotron mass m^* to free electron mass m_0. T_D is the Dingle temperature, and $\alpha = (2\pi^2 k_B m_0)/(\hbar e)$. The oscillations are described by the sine term with a phase factor $\gamma - \delta$, where $\gamma = \frac{1}{2} - \frac{\phi_B}{2\pi}$ and ϕ_B is the Berry phase. The phase shift δ is determined by the dimensionality of the Fermi surface and takes a value of 0 for 2D or $\pm 1/8$ for 3D cases.

From the LK formula, the effective mass m^* can be obtained from the fit of the temperature dependence of the oscillation amplitude by the thermal damping factor R_T. Because the FFT amplitude is used for the fit, the inverse field $1/B$ in R_T is taken as the average inverse field $1/\bar{B}$, defined as $1/\bar{B} = (1/B_{max} + 1/B_{min})/2$, where B_{max} and B_{min} define the magnetic field range used for the FFT. We have extracted nearly zero effective masses from the FFT analyses in the 5–31 T field range, i.e. $(0.024 \pm 0.001)m_0$, $(0.022 \pm 0.001)m_0$, $(0.041 \pm 0.001)m_0$, and $(0.051 \pm 0.0008)m_0$ for the α, β, γ and ε bands respectively, which fall into the range of the known topological semimetals [37]. For the η band with the highest frequency, a reliable fit is not possible, since the η-FFT amplitude damps out quickly with increasing temperature and there are only limited data points (see figure 2(a)). Moreover, there are another two additional frequencies near 400 T. Since their FFT amplitudes are also quickly damped with increasing temperature, we did not include them in our detailed analyses.

It is worthy to point out that the estimated values of effective mass from the FFT analyses are dependent on the field range to some extent. For instance, if we shrink the field range to 20 T–31 T where we can do FFT analyses only for the γ and ε oscillation components, but not for the α and β components which exhibit only a half oscillation peak, the fitted effective mass increases, up to ~0.28–0.30m_0. Although the variation of the extracted effective mass with the field range in the FFT analyses brings in an uncertainty for the fitted effective mass, it is only the approach to estimate effective mass when multiple oscillations frequencies are close to each other (which is the case for $CaSn_3$). Since clear oscillation peaks with the γ and ε frequencies extend to 5 T, we think the FFT analyses covering a wider field range (down to 5 T) give more accurate effective masses. For the quantum oscillations with single frequency, the effective mass can generally be obtained simply by fitting the temperature dependence of one oscillation peak

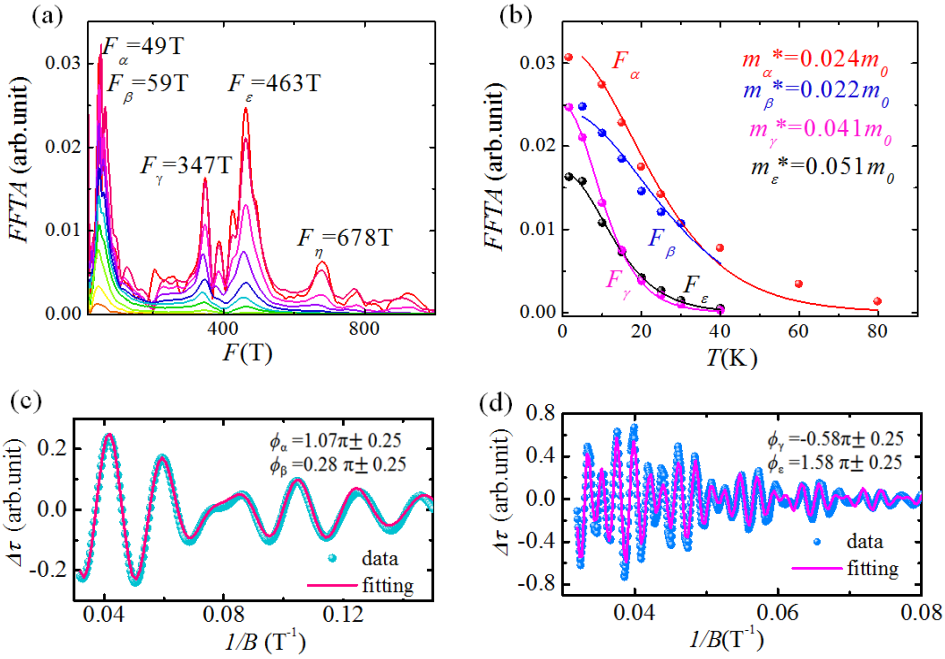

Figure 2. (a) The FFT of the oscillatory magnetic torque $\Delta\tau$ for B//[1 0 0]. (b) The temperature dependences of the FFT amplitudes for the four major frequencies; the solid lines represent the fits to the LK formula. (c) Low frequency (F_α and F_β) oscillatory components of magnetic torque obtained after filtering the high-frequency components. (d) High frequency (F_γ and F_ε) oscillatory components of magnetic torque obtained after filtering the low-frequency components. The solid curves in (c) and (d) represent the fits of the $T = 1.6$ K oscillation patterns by the two-band LK formula.

height at a finite field. However, such a method is not applicable for $CaSn_3$, since it shows multiple oscillation frequencies, with γ and ε (or α and β) being too close.

In addition to light effective mass, high quantum mobility and π Berry phase are also important characteristics of relativistic fermions. For the multi-frequency oscillations seen in $CaSn_3$, these parameters cannot be directly obtained through the conventional approaches (i.e. the Dingle plot and the Landau level fan diagram) but can be extracted through a fit of the oscillation pattern to the multiband LK formula, which is generalized from the single band LK model (equation (1)). This method has been shown to be efficient for the analyses of multi-frequency quantum oscillations in several topological semimetal systems [37–40]. With the effective masses and oscillation frequencies being the known parameters, we can fit the dHvA oscillation patterns at 1.6 K by the multiband LK formula. In order to achieve more accurate fits, we have separated the low frequency oscillation components (F_α and F_β) from the high frequency components (F_γ and F_ε) and fit them individually. The highest frequency (F_η) component, however, has been filtered out since an accurate effective mass cannot be obtained as stated above. As shown in figures 2(c) and (d), the two-band LK-formula fits both the low- and high-frequency oscillation patterns very well, yielding Dingle temperature T_D of 25, 60, 67, and 75 K for the α, β, γ and ε bands, respectively. From T_D, we can further derive quantum relaxation time $\tau_q = \hbar/(2\pi k_B T_D)$ and quantum mobility $\mu_q = e\tau/m^*$. The obtained values of μ_q are 4278, 1188, 779, and 528 cm^2 V^{-1} s^{-1} for α, β, γ and ε bands, respectively. From these multiband LK-fits, we have also determined the phase factor -γ-δ as well as the Berry phase ϕ_B for each band. Owing to the 3D characteristic of these bands as shown below, the phase shift δ takes value of $\pm 1/8$ as mentioned above. With this consideration, the Berry phases derived from our analyses are $(1.07 \pm 0.25)\pi$, $(0.28 \pm 0.25)\pi$, $(-0.58 \pm 0.25)\pi$ and $(1.58 \pm 0.25)\pi$ for the α, β, γ and ε bands, respectively (the errors of the fitted Berry phases for α, β, γ and ε bands are all in the range of 0.02–0.04π). The Berry phases for the α and ε bands are close to the ideal value of π. This result, combined with the nearly zero cyclotron mass derived from the temperature dependence of oscillation amplitude, implies relativistic nature of the electrons hosted by these bands.

We have further measured the angular dependences of the quantum oscillations to reveal the Fermi surface morphology of $CaSn_3$. As shown in figure 3(a), the oscillation patterns display a clear evolution with the change of field orientation angle from the [1 0 0] (defined as $\theta = 0°$) to [0 1 0] ($\theta = 90°$) direction (see the inset of figure 3(a) for the measurement setup). Figure 3(b) summarizes the angular dependence of the major frequencies, obtained from the FFT analyses of the oscillation patterns shown in figure 3(a). All of the five major frequencies, F_α, F_β, F_γ, F_ε and F_η, have been probed for all field orientations. Additionally, we have probed two frequency components F_λ and F_κ, when the field is not aligned close to the [1 0 0] and [0 1 0] directions. The angular dependences of all these frequencies display nearly symmetric patterns with respect to [1 1 0] ($\theta = 45°$) [i.e. $F(\theta) \approx F(90° - \theta)$], in agreement with the cubic symmetry of $CaSn_3$. These results clearly indicate a 3D Fermi surface for $CaSn_3$.

Although [35] has reported the calculated Fermi surface of $CaSn_3$ and found it is extremely complex and consists of a number of pockets, no quantitative information on the sizes

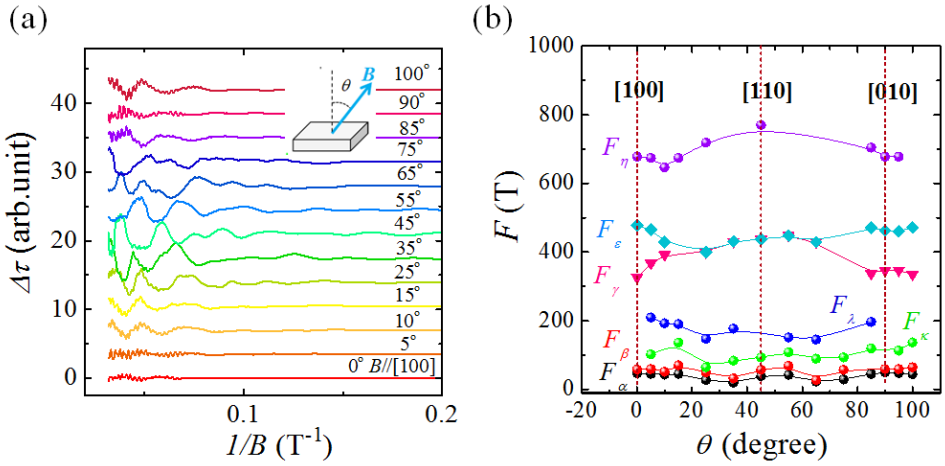

Figure 3. (a) dHvA oscillations of $CaSn_3$ at $T = 1.6$ K under different magnetic field orientations. Inset: the experimental setup. The data of different θ have been shifted for clarity. (b) The angular dependence of oscillation frequencies for $CaSn_3$. The vertical dashed lines mark specific crystallographic directions.

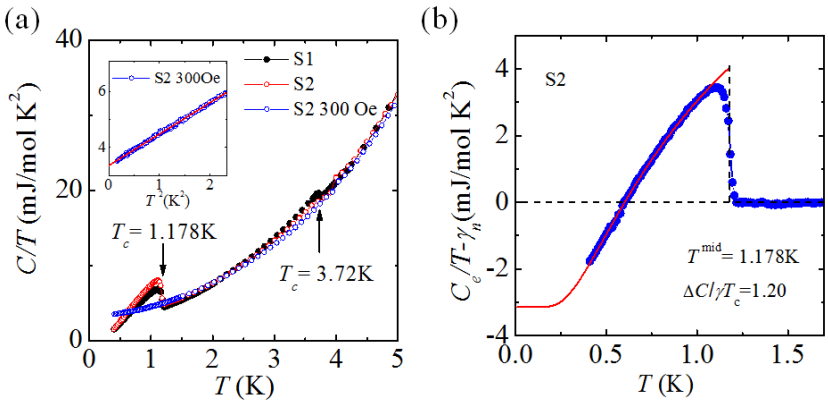

Figure 4. (a) Temperature dependence of specific heat $C(T)/T$ for two $CaSn_3$ single crystal samples. Sample 2 is fresher than sample 1 since it was exposed to air only for a very short period of time. We also measured sample 2 under a magnetic field of 300 Oe (applied along the [1 0 0] direction) Inset: $C(T)/T$ versus T^2 at low temperatures for sample 2 measured under the field of 300 Oe. The red line shows the linear fit to $C(T)/T = \gamma_n + \beta T^2$, from which the normal-state Sommerfeld coefficient γ_n is estimated to be 3.36 mJ (mol $K^2)^{-1}$. (b) Electronic specific heat $C_e(T)/T$ as a function of temperature after subtracting γ_n. The red solid curve represents the fit to single-band isotropic *s*-wave BCS model; the entropy balance between superconducting and normal state at T_c is maintained for this fit.

of the pockets is given. Therefore, we are unable to make quantitative comparison between our experimental results and the calculated Fermi surfaces. But, qualitatively, the quantum oscillation frequencies probed in our experiments are consistent with the calculated Fermi surface. Specifically, those lower oscillation frequencies (i.e. F_α, F_β, F_κ and F_λ) are likely to correspond to those small/point-like Fermi surfaces shown in figures 4(c) and (e) in [35], while those higher frequencies (i.e. F_γ, F_ε and F_η) might correspond to those larger Fermi pockets centered around the Brillouin zone center and boundaries (figures 4(a) and (d) in [35]).

3.2. Intrinsic superconductivity at 1.178 K in $CaSn_3$

In addition to topological fermion properties, $CaSn_3$ also exhibits intrinsic superconductivity below 1.178 K. As shown in figure 4, we observed a significant superconducting transition peak near 1.2 K in specific heat. $CaSn_3$ was previously reported to be superconducting with $T_c^{onset} \sim 4.2$ K [35], which appears to contradict our result. However, our detailed studies show that the $T_c^{onset} \sim 4.2$ K superconductivity, which is also clearly seen in our specific data for one of the measured samples (i.e. a small specific heat peak at 3.72 K in sample 1, as denoted an arrow in figure 4(a)), is not an intrinsic property of $CaSn_3$, but results from an impurity phase of Sn present on the sample surface, as has been clearly demonstrated in supplementary material. Such surface Sn impurities should be attributed to the surface decomposition of the air sensitive $CaSn_3$ and is responsible for the superconducting transition near 3.72 K in specific heat. When we measured a fresh sample which was exposed to air for a very short period of time (i.e. sample 2 in figure 4), we found that the specific heat anomaly near 3.72 K due to the superconductivity of Sn on the sample surface became very weak. From the susceptibility data shown in supplementary figure S3(a), the superconducting volume fraction of Sn is estimated to be ~2.4%. Additionally, we also conducted specific heat measurements under a magnetic field of 300 Oe for sample 2 and found its superconductivity at

1.178 K is fully suppressed by this magnetic field, suggesting it its upper critical field is less than 300 Oe.

By subtracting the specific data taken at 300 Oe from the zero-field data, we have obtained the intrinsic superconducting electronic specific heat C_{es} of $CaSn_3$ for sample 2. The obtained data are presented in figure 4(b), which plots the temperature dependence of $C_e/T - \gamma_n$, where $\gamma_n = 3.36$ mJ (mol K^2)$^{-1}$ is the Sommerfeld coefficient of $CaSn_3$, obtained from the linear fit shown in the inset of figure 4(a) (note that $C_e/T - \gamma_n$ slightly deviates from zero above T_c (=1.178 K) due to the suppression of the superconductivity of impurity Sn on the sample surface by the magnetic field and we have offset it to zero for the BCS fit shown below). From an entropy-conserving construction (see the black dashed line in figure 4(b)), the midpoint transition temperature T_c^{mid} was estimated to be 1.178 K and the specific heat jump $\Delta C/T_c^{mid} = 4.03$ mJ (mol K^2)$^{-1}$. Using these parameters, $\Delta C/\gamma_n T_c^{mid}$ is estimated to be 1.20, close to the expected value of 1.43 for weak-coupling BCS superconductors, indicating $CaSn_3$ falls into this classification. Furthermore, the superconducting electronic specific heat of $CaSn_3$ can be well-fitted by the single-band isotropic *s*-wave BCS model (see the red fitted curve in figure 4(b)). The reduced gap magnitude $2\Delta/k_B T_c$ obtained from the fit is 3.40, close to the value of 3.53 expected for weak coupling BCS superconductors. The fitted Sommerfeld coefficient γ_n' is 3.15 mJ (mol K^2)$^{-1}$. Given that the γ_n value obtained from the linear fit in the inset of figure 4(a) is 3.36 mJ (mol K^2)$^{-1}$, the superconducting volume fraction of $CaSn_3$ is estimated to be $\gamma_n'/\gamma_n = 94\%$. Since γ_n (=3.36 mJ (mol K^2)$^{-1}$) is slightly overestimated due to the existence of tiny amount of Sn on the sample surface, the actual superconducting volume fraction should be above 94%.

4. Discussion

In general, the realization of TSC requires the presence of spin-polarized TSSs, i.e. Dirac-cone type surface states with helical spin polarization. The other requirement is a fully opened bulk superconducting gap. When these requirements are met, the TSC is manifested by a complex surface superconducting order parameter consisting of both spin-singlet and spin-triplet components. The spin-triplet component hosts Majorana fermions. From the above discussions, $CaSn_3$ appears to meet these requirements. As discussed above, our dHvA quantum oscillation studies clearly demonstrate the existence of relativistic fermions in this material, indicating the presence of non-trivial band topology in $CaSn_3$ and possible TSSs. Moreover, if its topological states are proven to be true, its polarized spins on surface should be aligned along the in-plane direction due to its centrosymmetric crystal structure [32], which should make the surface superconducting order parameter relatively simple. Additionally, the stoichiometric composition of $CaSn_3$ guarantees homogeneous superconductivity, which is a desired condition for probing Majorana surface modes. With these advantages, $CaSn_3$ might be an interesting candidate for a topological superconductor.

Although our specific heat data analyses for $CaSn_3$ suggest its bulk superconductivity can be fitted with s-wave pairing, it does not conflict with possible existence of TSC. In general, when SOC is strong, TSC can be generated from s-wave superconductors under certain situations. One well-known example is the TSC created in hybrid s-wave superconductor -semiconductor nanowire devices where the superconducting proximity effect plays a critical role as noted above [9–11]. The other recently established example is the TSC observed on the surface of an iron chalcogenide superconductor $FeTe_{0.55}Se_{0.45}$ [31]. While its bulk superconductivity is topologically trivial and can be described as a two-band, extended *s*-wave superconductor [41], its TSC is generated by the spin-helical surface states.

Finally, we would like to point out that $CaSn_3$ belongs to a large family of materials with $AuCu_3$-type structure, most of which are superconducting, such as La_3In (T_c =10.4 K) [42], $Sr_{1-x}Na_xBi_3$ ($T_c = 9$ K) [43], and YSn_3 ($T_c = 7$ K) [44]. The highest T_c among these compounds is about 10 K. Since the non-trivial band topology is determined by crystal symmetry, compounds isostructural to $CaSn_3$ may have similar band structure. We expect our work on $CaSn_3$ can inspire band structure studies on other $AuCu_3$-type compounds. If they are also proven to possess non-trivial band topology, they may become candidates of topological superconductors with higher T_c.

5. Conclusion

In summary, from dHvA quantum oscillation studies on $CaSn_3$ single crystal samples, we have found evidence for relativistic fermions in this material. Furthermore, we discovered that this material exhibits intrinsic superconductivity with T_c ~ 1.178 K. These findings suggest $CaSn_3$ can be used a platform to explore possible TSC. Further, our finding could also motivate the search for TSC in other members in the large material family with the $AuCu_3$-type structure and superconductivity.

Acknowledgments

This work was supported by the US Department of Energy (DOE) under Grant No. DE-SC0014208. The heat capacity measurements were performed by FNW and PWA with support from the US DOE under BES Grant No. DE-FG02-07ER46420. A portion of this work was performed at the NHMFL, which is supported by National Science Foundation Cooperative Agreement No. DMR-1157490 and the State of Florida.

ORCID iDs

Y L Zhu https://orcid.org/0000-0002-6692-1406

References

[1] Read N and Green D 2000 Paired states of fermions in two dimensions with breaking of parity and time-reversal symmetries and the fractional quantum Hall effect *Phys. Rev.* B **61** 10267

[2] Sato M and Ando Y 2017 Topological superconductors: a review *Rep. Prog. Phys.* **80** 076501

[3] Fu L and Kane C L 2008 Superconducting proximity effect and Majorana fermions at the surface of a topological insulator *Phys. Rev. Lett.* **100** 096407

[4] Xu S-Y *et al* 2014 Momentum-space imaging of cooper pairing in a half-Dirac-gas topological superconductor *Nat. Phys.* **10** 943

[5] Wang M-X *et al* 2012 The coexistence of superconductivity and topological order in the Bi_2Se_3 thin films *Science* **336** 52

[6] Xu J-P *et al* 2015 Experimental detection of a Majorana mode in the core of a magnetic vortex inside a topological insulator-superconductor $Bi_2Te_3/NbSe_2$ heterostructure *Phys. Rev. Lett.* **114** 017001

[7] Sau J D, Lutchyn R M, Tewari S and Das Sarma S 2010 Generic new platform for topological quantum computation using semiconductor heterostructures *Phys. Rev. Lett.* **104** 040502

[8] Lutchyn R M, Sau J D and Das Sarma S 2010 Majorana fermions and a topological phase transition in semiconductor-superconductor heterostructures *Phys. Rev. Lett.* **105** 077001

[9] Mourik V, Zuo K, Frolov S M, Plissard S R, Bakkers E and Kouwenhoven L P 2012 Signatures of Majorana fermions in hybrid superconductor-semiconductor nanowire devices *Science* **336** 1003–1007

[10] Rokhinson L P, Liu X and Furdyna J K 2012 The fractional a.c. Josephson effect in a semiconductor-superconductor nanowire as a signature of Majorana particles *Nat. Phys.* **8** 795

[11] Das A, Ronen Y, Most Y, Oreg Y, Heiblum M and Shtrikman H 2012 Zero-bias peaks and splitting in an Al–InAs nanowire topological superconductor as a signature of Majorana fermions *Nat. Phys.* **8** 887

[12] Sun H-H *et al* 2016 Majorana zero mode detected with spin selective Andreev reflection in the vortex of a topological superconductor *Phys. Rev. Lett.* **116** 257003

[13] He Q L *et al* 2017 Chiral Majorana fermion modes in a quantum anomalous Hall insulator–superconductor structure *Science* **357** 294

[14] Hor Y S, Williams A J, Checkelsky J G, Roushan P, Seo J, Xu Q, Zandbergen H W, Yazdani A, Ong N P and Cava R J 2010 Superconductivity in $Cu_xBi_2Se_3$ and its implications for pairing in the undoped topological insulator *Phys. Rev. Lett.* **104** 057001

[15] Wray L A, Xu S-Y, Xia Y, San Hor Y, Qian D, Fedorov A V, Lin H, Bansil A, Cava R J and Hasan M Z 2010 Observation of topological order in a superconducting doped topological insulator *Nat. Phys.* **6** 855–59

[16] Matano K, Kriener M, Segawa K, Ando Y and Zheng G 2016 Spin-rotation symmetry breaking in the superconducting state of $Cu_xBi_2Se_3$ *Nat. Phys.* **12** 852

[17] Aggarwal L, Gaurav A, Thakur G S, Haque Z, Ganguli A K and Sheet G 2016 Unconventional superconductivity at mesoscopic point contacts on the 3D Dirac semimetal Cd_3As_2 *Nat. Mater.* **15** 32–37

[18] Wang H, Wang H, Liu H, Lu H, Yang W, Jia S, Liu X-J, Xie X C, Wei J and Wang J 2016 Observation of superconductivity induced by a point contact on 3D Dirac semimetal Cd_3As_2 crystals *Nat. Mater.* **15** 38–42

[19] Zhang J L *et al* 2011 Pressure-induced superconductivity in topological parent compound Bi_2Te_3 *Proc. Natl Acad. Sci.* **108** 24

[20] He L, Jia Y, Zhang S, Hong X, Jin C and Li S 2016 Pressure-induced superconductivity in the three-dimensional topological Dirac semimetal Cd_3As_2 *Npj Quantum Mater.* **1** 16014

[21] Zhou Y *et al* 2016 Pressure-induced superconductivity in a three-dimensional topological material $ZrTe_5$ *Proc. Natl Acad. Sci.* **113** 2904

[22] Li Y *et al* 2017 Concurrence of superconductivity and structure transition in Weyl semimetal TaP under pressure *Npj Quantum Mater.* **2** 66

[23] Kang D *et al* 2015 Superconductivity emerging from a suppressed large magnetoresistant state in tungsten ditelluride *Nat. Commun.* **6** 7804

[24] Qi Y *et al* 2016 Superconductivity in Weyl semimetal candidate $MoTe_2$ *Nat. Commun.* **7** 11038

[25] Aggarwal L, Gayen S, Das S, Kumar R, Süß V, Felser C, Shekhar C and Sheet G 2017 Mesoscopic superconductivity and high spin polarization coexisting at metallic point contacts on Weyl semimetal TaAs *Nat. Commun.* **8** 13974

[26] Butch N P, Syers P, Kirshenbaum K, Hope A P and Paglione J 2011 Superconductivity in the topological semimetal YPtBi *Phys. Rev.* B **84** 220504

[27] Liu Z K, Yang L X, Wu S-C, Shekhar C, Jiang J, Yang H F, Zhang Y, Mo S-K, Hussain Z and Yan B 2016 Observation of unusual topological surface states in half-Heusler compounds LnPtBi (Ln = Lu, Y) *Nat. Commun.* **7** 12924

[28] Ali M N, Gibson Q D, Klimczuk T and Cava R J 2014 Noncentrosymmetric superconductor with a bulk three-dimensional Dirac cone gapped by strong spin-orbit coupling *Phys. Rev.* B **89** 020505

[29] Bian G *et al* 2016 Topological nodal-line fermions in spin-orbit metal $PbTaSe_2$ *Nat. Commun.* **7** 10556

[30] Guan S-Y, Chen P-J, Chu M-W, Sankar R, Chou F, Jeng H-T, Chang C-S and Chuang T-M 2016 Superconducting topological surface states in the noncentrosymmetric bulk superconductor $PbTaSe_2$ *Sci. Adv.* **2** e1600894

[31] Zhang P *et al* 2018 Observation of topological superconductivity on the surface of an iron-based superconductor *Science* **360** 182

[32] Sakano M, Okawa K, Kanou M, Sanjo H, Okuda T, Sasagawa T and Ishizaka K 2015 Topologically protected surface states in a centrosymmetric superconductor β-$PdBi_2$ *Nat. Commun.* **6** 8595

[33] Kim H *et al* 2018 Beyond triplet: unconventional superconductivity in a spin-3/2 topological semimetal *Sci. Adv.* **4** eaao4513

[34] Gupta S, Juneja R, Shinde R and Singh A K 2017 Topologically nontrivial electronic states in $CaSn_3$ *J. Appl. Phys.* **121** 214901

[35] Luo X, Shao D F, Pei Q L, Song J Y, Hu L, Han Y Y, Zhu X B, Song W H, Lu W J and Sun Y P 2015 Superconductivity in $CaSn_3$ single crystals with a $AuCu_3$-type structure *J. Mater. Chem.* C **3** 11432–8

[36] Mikitik G P and Sharlai Y V 1999 Manifestation of Berry's phase in metal physics *Phys. Rev. Lett.* **82** 2147

[37] Hu J *et al* 2016 Evidence of topological nodal-line fermions in ZrSiSe and ZrSiTe *Phys. Rev. Lett.* **117** 016602

[38] Hu J *et al* 2016 π Berry phase and Zeeman splitting of Weyl semimetal TaP *Sci. Rep.* **6** srep18674

[39] Hu J, Tang Z, Liu J, Zhu Y, Wei J and Mao Z 2017 Nearly massless Dirac fermions and strong Zeeman splitting in the nodal-line semimetal ZrSiS probed by de Haas–van Alphen quantum oscillations *Phys. Rev.* B **96** 045127

[40] Hu J, Zhu Y, Gui X, Graf D, Tang Z, Xie W and Mao Z 2018 Quantum oscillation evidence for a topological semimetal phase in ZrSnTe *Phys. Rev.* B **97** 155101

[41] Hu J, Liu T J, Qian B, Rotaru A, Spinu L and Mao Z Q 2011 Calorimetric evidence of strong-coupling multiband superconductivity in $Fe(Te_{0.57}Se_{0.43})$ single crystal *Phys. Rev.* B **83** 134521

[42] Matthias B T, Compton V B and Corenzwit E 1961 Some new superconducting compounds *J. Phys. Chem. Solids* **19** 130

[43] Iyo A *et al* 2015 Large enhancement of superconducting transition temperature of $SrBi_3$ induced by Na substitution for Sr *Sci. Rep.* **5** 10089

[44] Kawashima K, Maruyama M, Fukuma M and Akimitsu J 2010 Superconducting state in YSn_3 with a $AuCu_3$-type structure *Phys. Rev.* B **82** 094517